UPPSALA
UNIVERSITET

Department of Physics and Astronomy

1FA195, Project in Physics and Astronomy

Final Report

Author:
Lucas Baldo Mesa Casa

Supervisor:
Jorge Cayao

July 14, 2020

Abstract

Nanowires with Rashba spin-orbit coupling represent a promising platform for the realization of one-dimensional topological superconductivity and Majorana bound states. In this work we investigate Majorana bound states in hybrid normal-superconductor and short superconductor-normal-superconductor junctions based on nanowires with Rashba spin-orbit coupling. In particular, we explore consequences of the topological phase transition as well as the non-locality and self conjugation properties of the Majorana states on the low-energy spectrum and the Josephson effect in the case of superconductor-normal-superconductor junctions. Our work shows the great potential of hybrid junctions as a platform for the study of topological superconductivity and Majorana bound states.

Acknowledgements

I would like to thank everyone in Annica Black-Schaffer's research group at Uppsala University, in particular Annica herself, Jorge Cayao and Oladunjoye Awoga for all their guidance and support.

I also acknowledge the financial support given by the European Commission through the Swedish Council for Higher Education in the framework of Erasmus+ KA107, which made possible the Master's exchange program to Uppsala University and by consequence the development of this project.

Contents

1 Introduction

Topological materials are a new class of condensed matter systems with unique properties that have attracted significant interest [1], specially because they represent a new state of matter and also due to their potential use in fault tolerant quantum computation [2]. These exotic states appear after a topological phase transition in the bulk of the system which is accompanied by the emergence of surface or edge states at the system's boundaries [1]. This relation is known as the bulk-boundary correspondence. Examples of topological materials are topological insulators, Weyl and Dirac semimetals, topological superconductors, etc. Topological superconductors are of particular significance because they host Majorana quasiparticles which posses exotic properties [3].

Majorana states were first proposed by Ettore Majorana in 1937 as real solutions to the Dirac equation [4] and are described by Hermitian creation operators, meaning the particles are their own antiparticles. Although being first considered in the context of particle physics, it has been shown that zero-energy quasiparticles in topological superconductors exhibit the reality condition of the Majoranas predicted by Ettore Majorana. These exotic quasiparticles are also referred to as Majorana Bound States (MBSs). MBSs hold potential application in fault tolerant quantum computation due to their non-Abelian statistics [5].

The simplest model for topological superconductivity was first envisaged by Alexei Kitaev [6] in a one-dimensional setup. His model predicted the emergence of MBSs with their wavefunctions located at the ends of the nanowire which exponentially decay into the bulk. The fact that MBSs emerge spatially separated at the ends of the system, together with the reality condition, defines a non-local fermion. There is one unnatural requirement in this model, however: spin polarised p-wave superconductivity, which is a rare type of superconducting pairing and scarce in nature. Surprisingly, it was later shown that the Kitaev model can be engineered by using conventional ingredients that include nanowires with Rashba spin-orbit coupling in proximity to an s-wave superconductor where a magnetic field drives the system into a topological superconducting phase [7, 8].

The detection of MBSs has been shown to be possible by exploiting their intrinsic properties. They must emerge at zero energy, a feature that has led to a large number of theoretical and experimental studies [3, 7, 9] that reported zero bias conductance peaks as a signature of MBSs. All these studies are largely based on tunneling of electrons from a normal lead (N) to the superconductor (S) with a MBS, where a perfect Andreev reflection then leads to a quantized value of $2e^2/h$ for the conductance. This transport process highlights the need of hybrid junctions, such as the normal-superconductor (NS) junctions. NS junctions also offer the advantage of having tunable chemical potentials through the insertion of gates near the interface, which can then can control the transmission process.

Another type of hybrid junction that has generated interest is the superconductor-normal-superconductor (SNS), where a finite phase difference between the superconductors gives rise to the formation of Andreev Bound States (ABSs) due to Andreev reflection [10] on both interfaces. The ABSs are responsible for the transfer of Cooper pairs between superconductors, which then leads to a finite persistent supercurrent across the junction, an effect known as the Josephson effect [11]. In the presence of MBSs, supercurrents have been shown to exhibit anomalous and unique features, suggesting them as a powerful route for the detection of MBSs based on the Josephson effect [12, 13].

Motivated by the exposed above, in this work we study topological superconductivity and MBSs in junctions based on nanowires with Rashba spin-orbit coupling. In particular, by exploiting the intrinsic MBS properties, we search for signatures of MBSs in the low energy spectrum and supercurrents. For this purpose we perform numerical simulations with realistic material parameters.

2 Majoranas in nanowires with Rashba spin-orbit coupling

In this chapter we describe how MBSs emerge in Rashba nanowires, a promising platform for one-dimensional topological superconductivity [8, 7]. It was shown that the combination of Rashba spin-orbit coupling, an external Zeeman field and s-wave superconductivity in a 1D system leads to p-wave topological superconductivity. This system can be modeled by the following Bogoliubov-de Gennes (BdG) Hamiltonian [8, 7],

$$H_{BdG} = (-\hbar^2\partial_x^2/2m^* - \mu)\tau_z\sigma_0 - i\alpha_R\partial_x\tau_z\sigma_y + B\tau_z\sigma_x + \Delta\tau_y\sigma_y, \tag{1}$$

where m^* is the effective mass of the electron, μ is the chemical potential through the nanowire, α_R is the Rashba spin-orbit coupling strength, and Δ is the superconducting pair potential, taken here to be real. Although $B = g\mu_B\beta/2$ is the Zeeman energy, linear with the magnetic field β, we will through this report refer to B as the Zeeman field. The basis used is $\hat{\Psi}^\dagger = \left(\hat{c}_\uparrow^\dagger, \quad \hat{c}_\downarrow^\dagger, \quad \hat{c}_\uparrow, \quad \hat{c}_\downarrow\right)$, so that τ_i and σ_i are the ith-Pauli matrices in particle-hole and spin spaces, respectively.

In order to show and understand how the topological superconducting phase and MBSs emerge in Eq. (1), we proceed to study both its bulk and edge properties. The bulk of a system is a continuum of states that arises due to the translational symmetry of the material. This symmetry results in a conserved quantity, the wavenumber k along the direction of the wire, and allows us to study the system through dispersion relations in which the topological phase transition is represented by a gap closing and reopening. This is done in the first section below. In the second section of this chapter we turn to the edge states, which are discrete and require a finite sized system. Because of this the wavenumber is no longer a good quantum number and we must use a discretized model. For this case, besides a gap closing the topological phase transition should also be evidenced by zero energy states, for which we can analyze the spatial distribution.

2.1 Rashba nanowires: bulk properties

The Rashba nanowire has a more natural basis than the one used in Eq. (1), that is sometimes referred to as the helical basis and diagonalizes the system for zero superconductivity, with eigenvalues given by

$$\epsilon_\pm = \xi_k \pm \sqrt{B^2 + \alpha_R^2 k^2}. \tag{2}$$

Here k is the wavenumber and $\xi_k = \hbar^2k^2/2m^* - \mu$. We then wish to rewrite Eq. (1) using this helical basis and, by defining the quantities

$$\Delta_{++} = \frac{-i\alpha_R k\Delta}{\sqrt{B^2 + \alpha_R^2 k^2}}, \quad \Delta_{--} = \frac{i\alpha_R k\Delta}{\sqrt{B^2 + \alpha_R^2 k^2}}, \quad \Delta_{+-} = \frac{B\Delta}{\sqrt{B^2 + \alpha_R^2 k^2}}, \tag{3}$$

we get the matrix

$$H_{BdG} = \frac{1}{2}\begin{pmatrix} \epsilon_+ & 0 & \Delta_{++} & \Delta_{+-} \\ 0 & \epsilon_- & -\Delta_{+-} & \Delta_{--} \\ \Delta_{++}^* & -\Delta_{+-}^* & -\epsilon_+ & 0 \\ \Delta_{+-}^* & \Delta_{--}^* & 0 & -\epsilon_- \end{pmatrix}. \tag{4}$$

Notice how we now have intraband superconducting terms and, moreover, that they are are odd in k. These terms $(++, --)$ are associated with the *p-wave superconductivity* required by the Kitaev model, whereas the even terms $(+-)$ refer to the usual *s-wave superconductivity*. The eigenvalues of the complete superconducting system are then given by [8, 7]:

$$\pm E_\pm = \pm\left[\xi_k^2 + \alpha_R^2 k^2 + B^2 + \Delta^2 \pm 2\sqrt{B^2\Delta^2 + (B^2 + \alpha_R^2 k^2)\xi_k^2}\right]^{1/2} \tag{5}$$

It is noticeable the mirroring of energies around zero due to the imposed electron-hole symmetry of the BdG formalism. Also, if we set Δ to zero we recover Eq. (2). If we evaluate the above expression at $k = 0$ we get

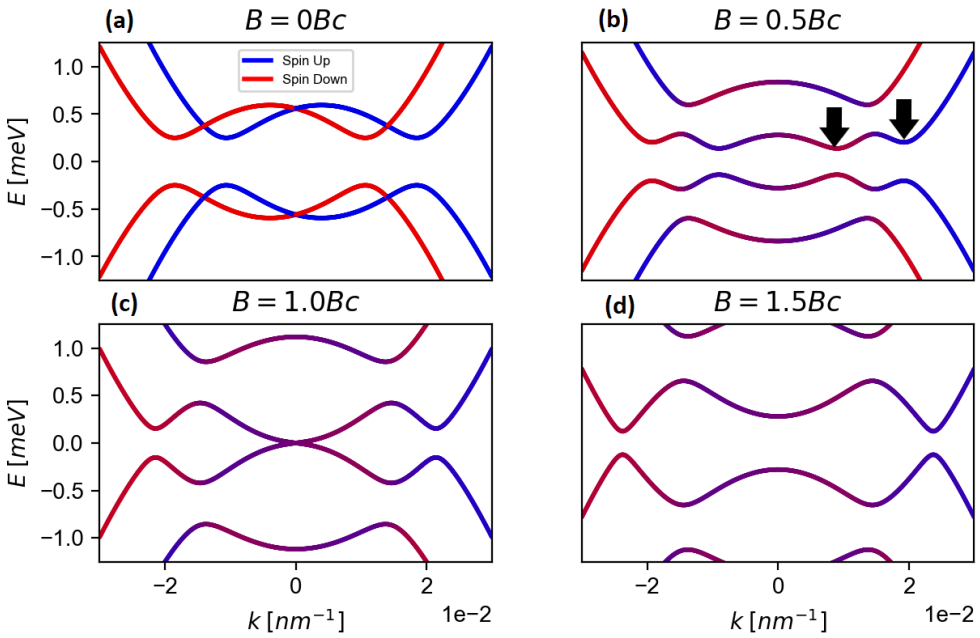

Figure 1: The dispersion relation of a nanowire for different values of the external field, with the spin projection along the Rashba axis shown by color. We study the case of zero field (a), $0.5B_c$ (b), $1.0B_c$ (c) and $1.5B_c$ (d). We note the gap closing in the $B = B_c$ case. The parameters used were $\Delta = 0.25$ meV, $\mu = 0.5$ meV and $\alpha_R = 20$ nm.meV, so that $B_c \approx 0.56$ meV.

$$\pm E_{\pm}(k = 0) = \pm|B \pm \sqrt{\Delta^2 + \mu^2}|. \tag{6}$$

From this it can be seen that the inner bands touch at zero energy for $k = 0$ when the field reaches a critical value,

$$B_c = \sqrt{\mu^2 + \Delta^2}. \tag{7}$$

This marks a gap closing and so is an evidence of a phase transition, which we will soon show is a topological one. To see this, we now plot these eigenvalues as a function of the wavenumber k using realistic parameter values and look for a gap closing by increasing the field in Fig. 1, where the field is given in units of the critical field B_c.

In Fig. 1(a) we have the dispersion for zero field. We observe that there are two distinct bands for positive energies, each with a definite spin value, evidenced by color. The parabolic bands are deformed around $k = 0$ due to the mixing of electron and hole bands through superconductivity, which generates a gap. We also point out the horizontal shift caused by the Rashba spin-orbit coupling, separating two distinct spin states. When we increase the field to $0.5B_c$, Fig. 1(b), we see that the different spins bands mix and we now have four non crossing bands, as well as two distinct gaps, indicated by arrows. As we further increase the field we see that the outermost bands are pushed further away into higher energies and at $B = B_c$, Fig. 1(c), the inner gap closes for $k = 0$. By increasing the field again the inner gap reopens and stays that way, Fig. 1(d). This is a signature of the topological phase transition we search for. In the topological phase the spin is strongly correlated with the wavenumber and this is sometimes referred to as spin-momentum locking. The outermost gap never closes and is not related to the topological phase transition and the outermost bands are pushed into higher energies as the field increases.

2.2 Rashba nanowires: edge properties

We have seen that the bulk of Rashba nanowires shows evidence of a topological phase transition and development of a topological phase. We will now demonstrate that in a finite sized system the topological phase is characterized by the presence of MBSs, which are exponentially localized on the edges of the nanowire [6].

By using a finite nanowire, the translational symmetry is broken, rendering k-space ineffective as a tool. Therefore we move on to the *Tight Binding* approach. This consists of discretizing real space and transforming the kinetic term as a hopping amplitude between different sites. Mathematically,

$$\hat{H}_{kin} = \int \sum_{\sigma} \hat{c}^{\dagger}_{x,\sigma} \left(\frac{-\hbar^2}{2m} \frac{\partial^2}{\partial x^2} - \mu(x) \right) \hat{c}_{x,\sigma} dx \rightarrow \sum_{i,\sigma} \hat{c}^{\dagger}_{\sigma}(x_i) \left(\frac{-\hbar^2}{2m} \frac{\delta^2}{\delta x_i^2} - \mu(x_i) \right) \hat{c}_{\sigma}(x_i). \tag{8}$$

The expressions for the first and second discrete derivatives are given by

$$\frac{\delta}{\delta x_i} \hat{c}_i = \frac{\hat{c}_{i+1} - \hat{c}_{i-1}}{2a}; \quad \frac{\delta^2}{\delta x_i^2} \hat{c}_i = \frac{\hat{c}_{i+1} - 2\hat{c}_i + \hat{c}_{i-1}}{a^2}, \tag{9}$$

where a is the lattice distance and we introduced the notation $\hat{c}_i = \hat{c}(x_i)$. Inserting this into the sum, we get

$$\hat{H}_{kin} = \sum_{i,\sigma} \left[(2t - \mu(x_i)) \hat{c}^{\dagger}_{i,\sigma} \hat{c}_{i,\sigma} - t \hat{c}^{\dagger}_{i,\sigma} (\hat{c}_{i+1,\sigma} + \hat{c}_{i-1,\sigma}) \right], \tag{10}$$

where $t = \hbar^2/2ma^2$ .For the SO coupling, using the expression above for the first order derivative, we find

$$\hat{H}_{SO} = \int \sum_{\sigma,\sigma'} \hat{c}^{\dagger}_{x,\sigma} \left(\sigma^y_{\sigma,\sigma'} \frac{-i\alpha_R}{2m} \frac{\partial}{\partial x} \right) \hat{c}_{x,\sigma'} dx \rightarrow \sum_i \frac{\alpha_R}{4ma} \left(\hat{c}^{\dagger}_{i,\downarrow} (\hat{c}_{i+1,\uparrow} - \hat{c}_{i-1,\uparrow}) - \hat{c}^{\dagger}_{i,\uparrow} (\hat{c}_{i+1,\downarrow} - \hat{c}_{i-1,\downarrow}) \right). \tag{11}$$

And for the Zeeman coupling:

$$\hat{H}_Z = \int \sum_{\sigma,\sigma'} \hat{c}^{\dagger}_{x,\sigma} \left(B\sigma^x_{\sigma,\sigma'} \right) \hat{c}_{x,\sigma'} dx \rightarrow \sum_i B \left(\hat{c}^{\dagger}_{i,\uparrow} \hat{c}_{i,\downarrow} + \hat{c}^{\dagger}_{i,\downarrow} \hat{c}_{i,\uparrow}) \right). \tag{12}$$

The case for superconductivity is rather trivial and very similar to the way the chemical potential term changes. First we make the transition from $k-$space into continuous position space and then, by making position space discrete, the superconductivity Hamiltonian becomes:

$$\hat{H}_{SC} = \frac{1}{2} \int \left[\Delta \left(\hat{c}^{\dagger}_{x,\uparrow} \hat{c}^{\dagger}_{x,\downarrow} - \hat{c}^{\dagger}_{x,\downarrow} \hat{c}^{\dagger}_{x,\uparrow} \right) + h.c. \right] dx \rightarrow \frac{1}{2} \sum_i \left[\Delta \left(\hat{c}^{\dagger}_{i,\uparrow} \hat{c}^{\dagger}_{i,\downarrow} - \hat{c}^{\dagger}_{i,\downarrow} \hat{c}^{\dagger}_{i,\uparrow} \right) + h.c. \right]. \tag{13}$$

It is important to notice that our basis for the *BdG* matrix can no longer be only 4-dimensional because the kinetic and SO terms mix operators with different values of x. In other words, we no longer have a parameter according to which we can evaluate the BdG Hamiltonians separately. Instead, we must construct one big matrix and diagonalize it all at once. This matrix will have dimensions $4N \times 4N$ ($2(spin) \times 2(particle - hole) \times N(sites)$) and we can assign to it the basis

$$\hat{\Psi}^{\dagger} = \begin{pmatrix} \hat{c}^{\dagger}_{1,\uparrow} & \hat{c}^{\dagger}_{1,\downarrow} & \hat{c}^{\dagger}_{2,\uparrow} & ... & \hat{c}^{\dagger}_{N,\downarrow} & \hat{c}_{1,\uparrow} & \hat{c}_{1,\downarrow} & \hat{c}_{2,\uparrow} & ... & \hat{c}_{N,\downarrow} \end{pmatrix}. \tag{14}$$

Thus, by defining the matrices

$$h = \begin{pmatrix} 2t - \mu & B \\ B & 2t - \mu \end{pmatrix}, \quad v = \begin{pmatrix} t & \alpha_R/4ma \\ -\alpha_R/4ma & t \end{pmatrix}, \quad \delta = \begin{pmatrix} 0 & \Delta \\ -\Delta & 0 \end{pmatrix} \tag{15}$$

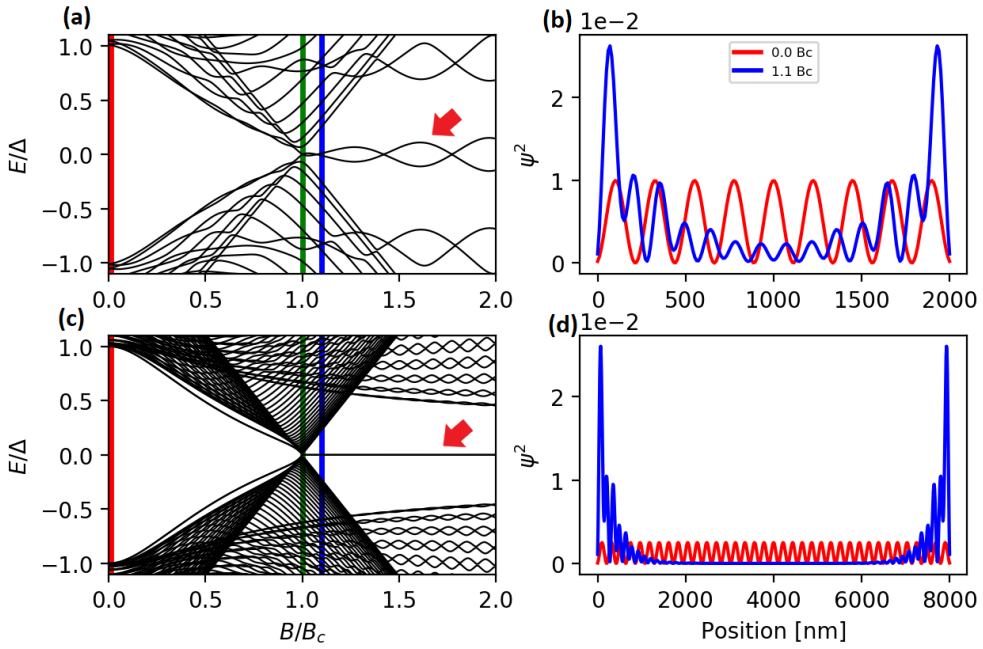

Figure 2: (a): energy spectrum as a function of the Zeeman field for a 2000 nm long Rashba nanowire. The green bar marks the critical field B_c for which there is a gap closing. In red and blue are marked zero and $1.1B_c$ values of the field for which we plot the lowest energy states wavefunction in (b). (c-d): the same plots for an 8000 nm Rashba nanowire. The parameters used were $\Delta = 0.25$ meV, $\mu = 0.5$ meV, $\alpha_R = 20$ nm.meV, $B_c \approx 0.56$ meV and $a = 10$ nm.

the final form of the BdG Hamiltonian is

$$H_{BdG} = \begin{pmatrix} h & v & 0 & .. & \delta & 0 & 0 & .. \\ v^\dagger & h & v & .. & 0 & \delta & 0 & .. \\ 0 & v^\dagger & h & .. & 0 & 0 & \delta & .. \\ : & : & : & : & : & : & : & : \\ \delta^\dagger & 0 & 0 & .. & -h^* & -v^* & 0 & .. \\ 0 & \delta^\dagger & 0 & .. & -v^T & -h^* & -v^* & .. \\ 0 & 0 & \delta^\dagger & .. & 0 & -v^T & -h^* & .. \\ : & : & : & : & : & : & : & : \end{pmatrix}. \tag{16}$$

On a side note, for the matrix above we chose open boundary conditions, which corresponds to a finite wire. However, by choosing periodic boundary conditions we could emulate an infinite wire. The only modification necessary for this would be to insert the elements v and $v^\dagger$ at the end points of the anti-diagonal of the first diagonal block and $-v^*$ and $-v^T$ for the second diagonal block.

Having now the tools to study these discrete systems we implement those models numerically and analyze the spectrum. In Fig. 2 we show in (a) and (c) plots of the energy levels as a function of the Zeeman field in units of the critical field B_c.

Fig. 2(a) corresponds to a 2000 nm long nanowire, where we observe a hard gap for low field values. As the Zeeman field increases the gap shortens, which is a consequence of the cooper pairs being destroyed by the field, until it closes at B_c, marked by a green stripe. This is the same value for which we observed a gap closing in the bulk of the system signaling a topological phase transition. At higher fields the gap reopens giving rise to a topological phase and a subgap state emerges with energy oscillating around zero. This state, which we highlight with an arrow, is the MBS and this oscillation was proposed as its signature

in zero-bias conductance measurements [14]. We can check that by looking at its spatial distribution across the nanowire, which is done in Fig. 2(b). The blue curve shows the wavefunction amplitude for the lowest lying state at a field of $1.1B_c$ as a function of the position along the 2000 nm nanowire. We observe that the curve peaks at the edges decaying exponentially towards the bulk of the system. For comparison, we show in red the lowest lying state for zero field and observe its delocalization. Both states have an oscillatory wavefunction, which is a result of finite superconductivity and a positive chemical potential. The two values of the field used are marked with stripes in the spectrum plot for reference.

Similarly, in Fig. 2(c-d) we have the spectrum (c) and wavefunctions (d) for a 8000 nm long nanowire. For this longer system we observe that the oscillations of the MBSs energies are reduced to the point they can be considered zero energy modes, as pointed by the arrow in Fig. 2(c). Because of this, these states are sometimes referred to as Majorana Zero Modes. This decrease in energy is due to the greater spatial separation between the two Majorana peaks and subsequent negligible overlap through the bulk, which can be seen in the blue curve in Fig. 2(d).

Although we do not show here we have reproduced similar results for different values of the chemical potential. The main difference observed is that negative values of the chemical potential eliminate the oscillations of the wavefunction along the wire.

We conclude here the study of the finite simple nanowire systems by underlining that we observed a gap closing and reopening characterizing a topological phase transition that separates a trivial from a topological phase. In the topological regime we have found states exponentially localized at the edges, which we identify as MBSs. Moreover, the decrease in energy oscillation of such states shows a crucial factor for producing Majorana Zero Modes, that is, if the nanowire is too short the two peaks will overlap significantly, resulting in a non-zero energy state. We now proceed to the treatment of hybrid structures with nanowires, called junctions.

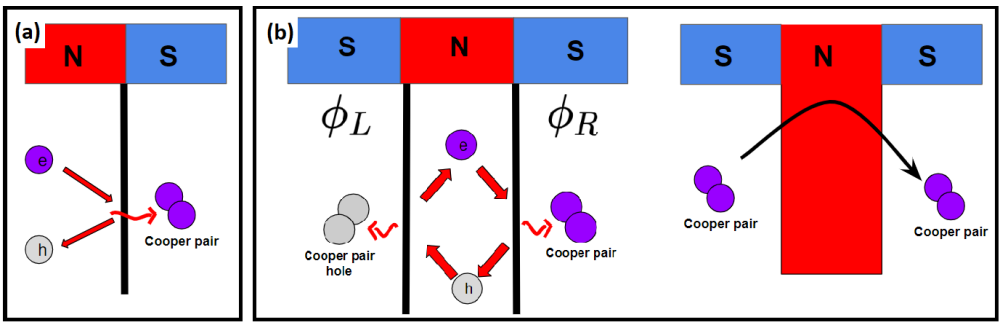

Figure 3: A sketch of the junctions considered and the important phenomena supported by them. In (a) is the NS junction and below it the Andreev reflection is depicted. In (b) we show a SNS junction with the cycle of Andreev reflections that generate an Andreev Bound State and a net transfer of Cooper pairs between the S regions.

3 Superconductor-semiconductor junctions in Rashba nanowires

So far we have considered homogeneous systems, where the parameters are constant throughout the whole nanowire. Many interesting phenomena involving Rashba nanowires, however, appear when considering hybrid structures [3]. These can be constructed by considering nanowires with spatially dependent parameters. For example, part of the nanowire can have its superconductivity taken away by removing the s-wave superconductor around it. These regions are denominated normal or normal-metal regions and we will use them to construct junctions. From the implementation point of view we simply set δ in Eq. (16) to zero for the corresponding sites.

We will consider two geometries. The first one, depicted in Fig. 3(a), is the NS junction and is comprised of a normal (N) region on one end of the nanowire and next to a superconducting (S) region. One interesting new phenomenon that occurs already is that an electron traveling in the N region and hitting the NS interface may get reflected as a hole instead of a usual electron. This process is called the Andreev reflection and it transfers a Cooper pair from the N into the S region [10, 15].

In a different case we instead remove the proximitized s-wave superconductor from the middle of the nanowire, leaving two separate S regions. This forms a SNS junction, Fig. 3(b), which also possesses interfaces between N and S regions and so supports Andreev reflections. Moreover, the hole generated in one of such reflections can hit the other interface and with the reverse process be reflected back as an electron. Multiple Andreev reflections result in the formation of an Andreev Bound State (ABS). This cycle of Andreev reflections is modulated by the superconducting phase and can result in a net current of Cooper pairs denominated a supercurrent [11], as we will discuss in the last section of this chapter.

3.1 NS junctions

It is important to understand the interactions between the 1D topological superconductors we have seen and non-superconducting N regions, as shown in Fig. 3(a), because these are present in the experimental settings related to the measurement of MBSs, such as the studies of zero bias conductance peaks [3]. That is why we briefly study here the behaviour of the NS junctions.

A NS junction can be modeled by putting the superconducting parameter to zero in one outer region of the nanowire while keeping the rest of the parameters constant. The size of this region has significant effect on the energy levels of the system and we are going to consider a nanowire with regions of equal proportions. By applying the above mentioned changes to the Hamiltonian of the system and numerically diagonalizing it for a 4000 nm long NS junction of equally sized regions we obtain the results shown in Fig. 4.

In Fig. 4(a) we show the energy spectrum as a function of the Zeeman field. As in the simple nanowire case we observe a gap closing and reopening at B_c, marked with a green stripe, with the emergence of low energy oscillating states at higher fields. This is a sign that there is still a topological phase transition

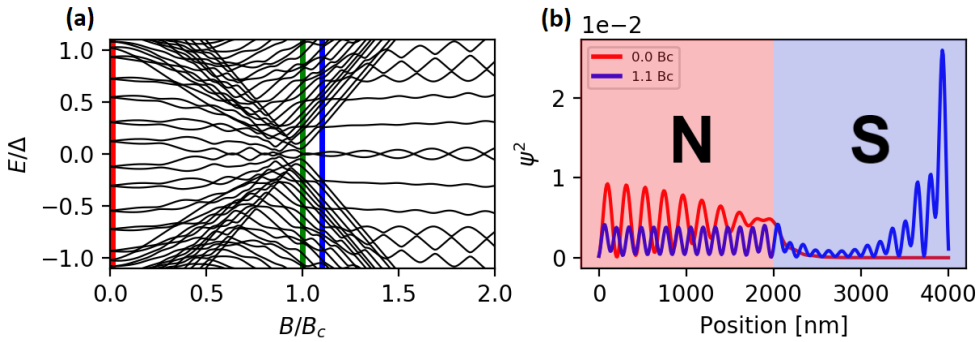

Figure 4: Panel (a): spectrum as a function of the Zeeman field. Marked in green is the critical field, which is the of the simple nanowire case. Panel (b): the wavefunctions of the lowest lying states for zero field (red) and $1.1B_c$ (blue). We have marked with stripes the field values for these states in the spectrum for reference. We point out that in the topological phase there is one Majorana peak in the outer edge of the S region, but the other peak is not present. This can be seen as the other Majorana leaking into the N region. The parameters used were $\mu = 0.5$ meV and $\alpha_R = 20$ nm.meV for the whole system with $\Delta = 0.25$ meV in the S region and $\Delta = 0$ in the N region.

happening in the system. The main differing features from the previous case are a smaller gap for higher fields and the presence of trivial finite-energy subgap states for low fields. These states originate from the N region, where the lack of superconductivity implies the lack of a gap. This can be checked by looking at the localization of such states, which we do in Fig. 4(b). In red we plot the wavefunction amplitude distribution across the system for the least energetic state at zero field. We see that it is indeed spread throughout the N region (left half of the structure) being virtually not present inside the S region (right half). In blue, on the other hand, we have plotted the wavefunction of the MBS at $1.1B_c$. We see that the outermost peak is still present and decaying exponentially towards the bulk, but the other peak, which we expected to find at the other end of the S region, is not there. This can be seen as the Majorana leaking into the N region and is a sign that the topological states are significantly influenced by the surroundings of the nanowire. This should be kept in mind when studying transport properties of these systems.

We have also considered NS junctions with parts of different proportions. We have observed that the features discussed above are still present, but the effects of the N region (such as the number of trivial subgap states) diminish as the region gets shorter. By contrast, when the S region is small the Majorana peaks overlap greatly and the energy of the MBSs becomes very large. If the S region is too small the gap does not reopen and the lowest lying states are not energetically separated from the others.

Having seen that there is an important interplay between a Rashba nanowire in the topological phase and its connecting non-topological regions, we move on to study a slightly more complex hybrid structure, the SNS junction.

3.2 SNS junctions

Differently from the structures so far discussed, SNS junctions present not only one S region, but two (see Fig. 3(b)). This gives importance to a parameter we have been ignoring so far, that is, the superconducting phase. The superconducting order parameter is in principle a complex quantity and its complex phase can be adjusted experimentally. By defining this phase for a given superconductor region labeled i as $\varphi_i = Arg(\Delta_i)$, the phase difference between the right and left S regions in a SNS junction is

$$\phi = \varphi_R - \varphi_L. \tag{17}$$

We will now study how the spectrum of short SNS junctions vary with respect to not only the Zeeman field, but also this phase difference. In Fig. 5 we present results for a junction with an extremely short N region of 20 nm length by fixing the Zeeman field to different values. For panels (a-d) we use outer S regions

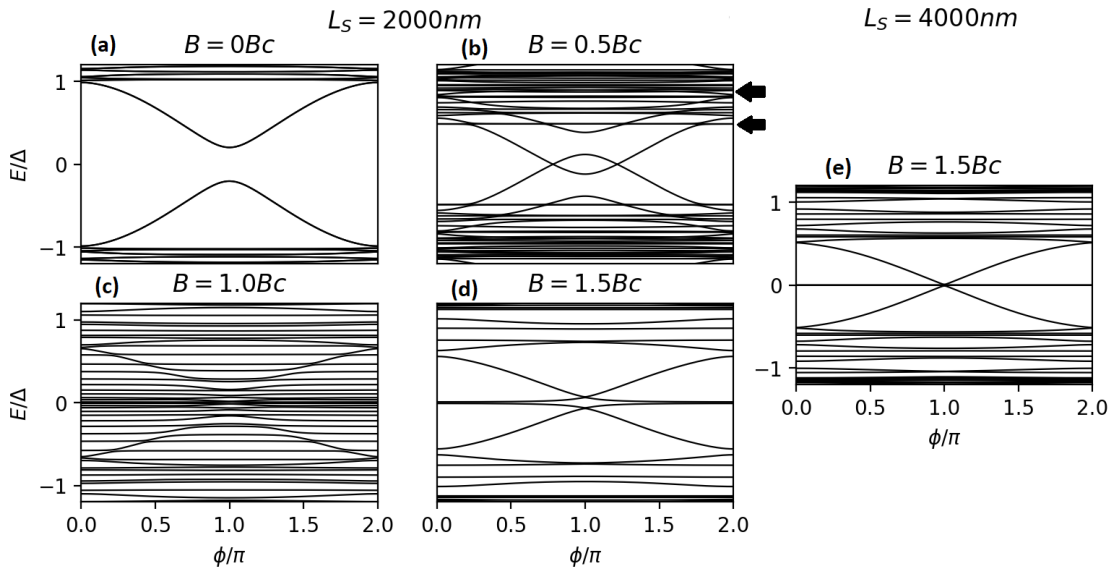

Figure 5: The energy spectrum, in units of the superconducting parameter, as a function of the phase difference, in units of π.

2000 nm long. In Fig. 5(a) we see the energy spectrum with respect to the phase difference in the absence of Zeeman field. We observe a gap, the size of the superconducting parameter as expected, throughout all the range of ϕ, but also a distinct subgap state. This state is close to the bulk in energy when ϕ is zero, but dips as this parameter increases, reaching a minimum close to zero energy at $\phi = \pi$. This state is the before mentioned ABS and it plays important roles in transport dynamics in SNS junctions, as we will see in the next section.

For now, in Fig. 5(b) we show the case for a field of $0.5B_c$. Here we observe that the MBS state we just discussed was actually degenerate and the presence of a Zeeman field split both curves, the bottom one dipping enough in energy to cross its electron-hole symmetric counterpart. Moreover we point out that there are two different gaps in the system, pointed by the black arrows. If we increase the field further up to its critical value $1B_c$ we obtain the results in Fig. 5(c). We see the closing of one of the gaps, just as in the previous systems, but also the presence of a phase-dependent state reaching a minimum at $\phi = \pi$. We also point out that the upper gap never closes and is not related to the topological phase transition. By driving the field up to $1.5B_c$, Fig. 5(d), we enter the topological regime and see a gap reopening, with a near zero energy state emerging, the MBS. Moreover, we see another subgap state appearing, with a shape similar to the ABS, and we observe this state pulls the MBS away from zero energy at $\phi = \pi$ and the two bands touch.

The energy splitting in the MBS bands at π is due to the finiteness of the S regions, as we can see by looking at Fig. 5(e). Here we see that the spectrum for a junction with 4000 nm long S regions does not present such a splitting, but instead the ABS-like bands cross at zero energy. We can better understand this behaviour by considering the localization of these states along the junction. This is done in Fig. 6, where we plot the wavefunctions amplitude along the nanowire.

In Fig. 6(a) we see that a lack of phase difference leads to a distribution closely related to a MBS in a simple nanowire, with one exponential peak at each end. By setting the phase difference to π we see this changes by the emergence of new bump in the middle of the nanowire, that is, at the junction. Closer inspection leads to identifying the bump as two distinct MBS peaks. With this in mind we can interpret the split in energy seen as resulting from a finite overlap of the new *inner* MBS peaks with the *outer* ones. This is consistent with the disappearance of the split for long enough S regions. From the point of view of the Kitaev model the finite phase difference separates the nanowire into two distinct topological domains, each

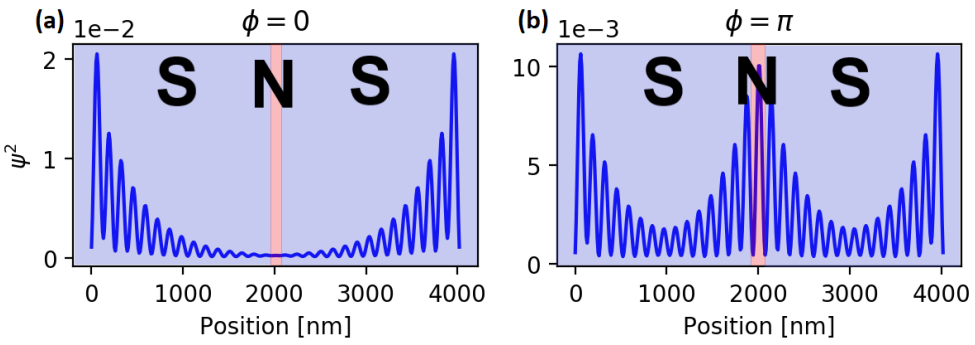

Figure 6: The wavefunction amplitude of the lowest lying state of a SNS junction along the nanowire. In (a) the case for zero phase difference is shown and distribution of the state is similar to a simple nanowire, with exponential localization at the edges. In (b) we have the case for a phase difference of π. Here we observe Majorana peaks not only at the edges but also at the junction, totaling four distinct peaks.

with MBS peaks at its edges.

We have seen that the presence of ABSs and the phase difference between the S regions change significantly the behaviour of the low energy spectrum of hybrid structures based on Rashba nanowires. We will now see some consequences of this in a phenomenon that can be measured experimentally, the Josephson supercurrent.

3.2.1 Josephson current

The cycle of Andreev reflections implied in ABSs leads to the transference of Cooper pairs from one S region to another, as is sketched in Fig. 3(b). In principle, the mirror symmetry of a SNS junction would guarantee that this process happens as frequently as its inverse. However, as we have seen in the last section, there is a parameter in the system that breaks this mirror symmetry, the superconducting phase difference. As a consequence, this phase can give preference to the flow of Cooper pairs in a certain direction. This is the well known Josephson Effect [11] and leads to a measurable supercurrent across the junction. For our system this supercurrent can be calculated through [15]

$$I(\phi) = -\frac{e}{h}\sum_{p>0}\frac{dE_p}{d\phi}, \tag{18}$$

where E_p represents phase-dependent energy levels and the sum is over positive-valued states only. Using this we can study how the current behaves in SNS junctions made with Rashba nanowires. This is done in Fig. 7, where we plot the supercurrent as a function of the phase for fixed values of the Zeeman field. In Fig. 7(a) we consider S regions with a length of 2000 nm. For zero field (red) the supercurrent shows a sinusoidal behaviour characteristic of the Josephson current. As the field becomes finite and increases (black, green and blue) we observe a reduction of the current amplitude, which is due to the decrease in effective superconductivity caused by the interplay between Cooper pairs and magnetic fields. The only distinct feature observed is a step-like curve for finite fields in the trivial phase (black), which is due to the ABSs crossing observed in the spectrum in Fig. 5(b).

In Fig. 7(b) we have the corresponding curves for a junction with 4000 nm long S regions. We observe similar results for fields up to the critical one (green), but a distinctly new behaviour in the topological phase (blue). We see that the supercurrent loses its sinusoidal character to increase linearly up to $\phi = \pi$, where it drops sharply to a negative value and continues to linearly increase. The fact that this change happened by increasing system length is a sign that it is related to non-local phenomena. This is referred to as a saw-tooth profile and is generated by the MBS peaks located at the junction [16]. This can be verified by looking at

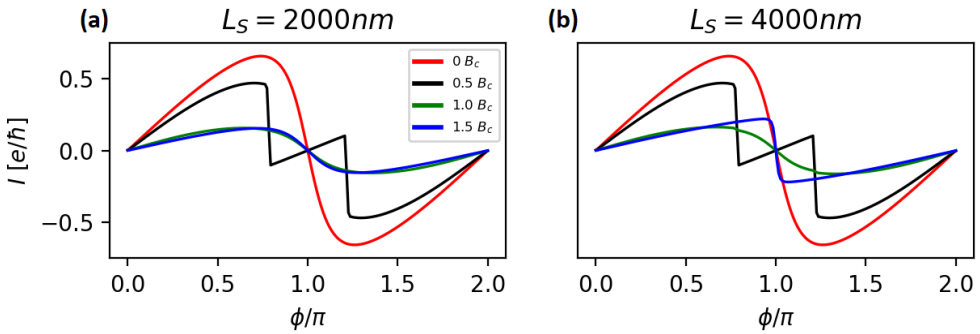

Figure 7: The supercurrent as a function of the phase difference for fixed Zeeman field and for S regions 2000 nm (left) and 4000 nm long (right). The zero field curves (red) follow sine-like behaviour and have maximum amplitude. As the field increases the amplitude diminishes (black, green and blue) and in the trivial phase (black) there is a step-like behaviour due to ABS crossings. For the longer system we observe the topological phase (blue) has a peculiar saw-tooth shape.

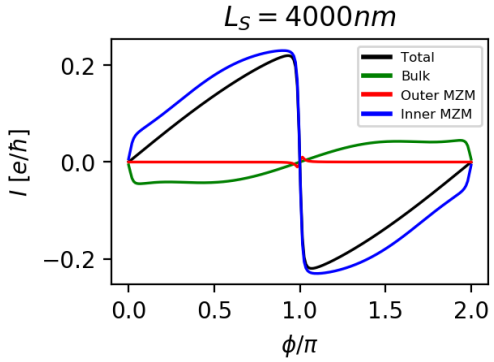

Figure 8: The contributions to the supercurrent as a function of phase difference for a SNS junction with 4000 nm long S regions. We observe the contribution from the outer MBS (red) is negligible, while the contributions from the bulk (green) is small and negative. We see that the inner MBS (blue) contributes the most towards the total (black) and is responsible for the saw-tooth shape.

the different contributions to this curve. In Fig. 8 we compare the contributions made by different states. The outer MBS (red) has virtually zero influence on the supercurrent. The bulk, or quasi-continuum, states (green) have a small and negative contribution. Finally we see that the inner MBS (blue), that is, the one localized at the junction, is responsible for the saw-tooth shape and overall contributes the most to the total supercurrent (black).

As we have seen, the Josephson supercurrent in SNS junctions can be calculated from the spectrum and the presence of MBSs at the junction affects the supercurrent in a unique way. This enables the use of the supercurrent profile as a signature detection of MBSs. Moreover, the dependence of the profile on the length of the superconductors is evidence on itself of the non-locality of the MBSs.

4 Conclusions and outlook

Through the study of both bulk and edge properties of nanowires with Rashba spin-orbit coupling, we have seen these systems present a topological phase transition at a critical field characterized by a gap closing and reopening and, for finite nanowires, the emergence of non-local low energy states in the topological phase that are exponentially localized at edges. These states were identified as the MBSs and they become Majorana Zero Modes when the nanowire is long enough.

By implementing hybrid structures we have seen that the presence of N regions inserts subgap states at low fields but the phase transition still present, although with a smaller gap in the topological phase. In a NS junction the MBS emerges in the S region with only its outer peak visible, the other leaking and spreading into the N region. In short SNS junctions the topological phase transition was observed, but we also have seen the appearance of ABSs as subgap states already in the trivial regime. We studied the effects of the phase difference between the S regions and have seen that when this difference equals π the Majorana Zero Mode gains a finite energy and becomes degenerate with the ABS, which in turn becomes a MBS. Looking at the wavefunctions of these states we see two Majorana peaks at the outer edges and two around the junction. These internal peaks became important when studying the Josephson current in the SNS junctions. We have seen that this current presents a sinusoidal behaviour with the phase difference and a drop in amplitude with the Zeeman field, but also a peculiar saw-tooth profile for long systems in the topological regime. By separating the different contributions to the current we have isolated the inner MBS as the source of this behaviour. This phenomenon serves as tool to detect the presence of MBSs and its dependence with the system length is evidence of the non-locality of these states.

Understanding the usefulness of hybrid junctions in the study of MBSs, we are now working on a new direction with a novel geometry involving several Rashba nanowires. This setup still holds experimental relevance and we aim to understand how to properly identify identify MBSs through its non-local property and using the tools we have studied here, such as detecting the gap closing.

References

[1] B.A. Bernevig and T.L. Hughes. *Topological Insulators and Topological Superconductors*. Princeton University Press, 2013.

[2] Chetan Nayak, Steven H. Simon, Ady Stern, Michael Freedman, and Sankar Das Sarma. Non-abelian anyons and topological quantum computation. *Rev. Mod. Phys.*, 80:1083–1159, 2008.

[3] Ramón Aguado. Majorana quasiparticles in condensed matter. *Nuovo Cimento*, 40:523–593, 2017.

[4] E. Majorana. Symmetrical theory of the electron and the positron. *Nuovo Cimento*, 5:171–184, 1937.

[5] Sankar Das Sarma, Michael Freedman, and Chetan Nayak. Majorana zero modes and topological quantum computation. *npj Quantum Information*, 1, 2015.

[6] A Yu Kitaev. Unpaired majorana fermions in quantum wires. *Physics-Uspekhi*, 44:131–136, 2001.

[7] Roman M. Lutchyn, Jay D. Sau, and S. Das Sarma. Majorana fermions and a topological phase transition in semiconductor-superconductor heterostructures. *Phys. Rev. Lett.*, 105:077001, 2010.

[8] Yuval Oreg, Gil Refael, and Felix von Oppen. Helical liquids and majorana bound states in quantum wires. *Phys. Rev. Lett.*, 105:177002, 2010.

[9] E. Prada, P. San-Jose, M. W. A. de Moor, A. Geresdi, E. J. H. Lee, J. Klinovaja, D. Loss, J. Nygård, R. Aguado, and L. P. Kouwenhoven. From andreev to majorana bound states in hybrid superconductor-semiconductor nanowires. arXiv:1911.04512, 2019.

[10] A.F. Andreev. The thermal conductivity of the intermediate state in superconductors. *JETP*, 19:1228, 1964.

[11] B.D. Josephson. The discovery of tunnelling supercurrents. *Rev. Mod. Phys.*, 46:251–254, 1974.

[12] Jorge Cayao. *Hybrid superconductor-semiconductor nanowire junctions as useful platforms to study Majorana bound states*. PhD thesis, Universidad Autónoma de Madrid, 2017. [arXiv:1703.07630].

[13] Oladunjoye A. Awoga, Jorge Cayao, and Annica M. Black-Schaffer. Supercurrent detection of topologically trivial zero-energy states in nanowire junctions. *Physical Review Letters*, 123, 2019.

[14] S. Das Sarma, Jay D. Sau, and Tudor D. Stanescu. Splitting of the zero-bias conductance peak as smoking gun evidence for the existence of the majorana mode in a superconductor-semiconductor nanowire. *Physical Review B*, 86, 2012.

[15] C. W. J. Beenakker. Three "universal" mesoscopic josephson effects. In *Transport Phenomena in Mesoscopic Systems*, pages 235–253, Berlin, Heidelberg, 1992.

[16] Jorge Cayao, Annica M Black-Schaffer, Elsa Prada, and Ramón Aguado. Andreev spectrum and supercurrents in nanowire-based sns junctions containing majorana bound states. *Beilstein Journal of Nanotechnology*, 9:1339–1357, 2018.